AIP Advances

RESEARCH ARTICLE | OCTOBER 06 2025

Fluorine doping of barium bismuthate by SF_6 plasma

L. Ceccon ; I. Ahmed ; M. Kaviani ; J. Van de Vondel ; G. Pourtois ; C. Merckling

AIP Advances 15, 105109 (2025)
https://doi.org/10.1063/5.0283535

19 March 2026 09:41:09

Fluorine doping of barium bismuthate by SF_6 plasma

Cite as: AIP Advances 15, 105109 (2025); doi: 10.1063/5.0283535
Submitted: 18 June 2025 • Accepted: 16 September 2025 •
Published Online: 6 October 2025

View Online Export Citation CrossMark

L. Ceccon,[1,2,a)] I. Ahmed,[1,2] M. Kaviani,[1] J. Van de Vondel,[3] G. Pourtois,[1] and C. Merckling[1,2]

AFFILIATIONS

[1] Imec, Kapeldreef 75, 3001 Leuven, Belgium
[2] Department of Materials Engineering, KU Leuven, Kasteelpark Arenberg 44, 3001 Leuven, Belgium
[3] Department of Physics and Astronomy, KU Leuven, Celestijnenlaan 200d, 3001 Leuven, Belgium

[a)] Author to whom correspondence should be addressed: Luca.Ceccon@imec.be

ABSTRACT

Topological insulators (TIs) are materials with an insulating bulk and topologically protected conductive surface states. Many potential applications can be found in the literature for this class of materials. However, the small bandgap and the poor stability of the TIs extensively studied in the literature, such as Bi_2Se_3 and Bi_2Te_3, restrict their potential. One of the proposed alternatives is barium bismuthate (BBO), an oxide perovskite that is predicted to be a TI with a relatively large bandgap of about 0.7 eV. Despite the potential of this material, accessing its TI phase requires increasing the Fermi energy by ~2 eV, and, to our knowledge, this has not yet been achieved experimentally. One proposed way to shift the Fermi energy is to substitute a part of the oxygen atoms in its structure with fluorine. In this study, we investigated the low-temperature fluorination of MBE-grown BBO thin films using SF_6 plasma as a fluorine source. We began our study by using XRD and AFM to identify the processing conditions that allowed us to preserve the quality of the film. Then, we confirmed the incorporation of fluorine into the exposed thin film by XPS and SIMS. Since oxygen deficient films are expected to be easier to alloy, we also compared these results with the fluorination of oxygen-deficient BBO_{3-x} films. Finally, we used DFT to demonstrate that the fluorination of BBO_3 is an energetically favorable process, supporting our observations.

© 2025 Author(s). All article content, except where otherwise noted, is licensed under a Creative Commons Attribution (CC BY) license (https://creativecommons.org/licenses/by/4.0/). https://doi.org/10.1063/5.0283535

19 March 2026 09:41:09

I. INTRODUCTION

Topological insulators (TIs) are materials characterized by an insulating bulk and topologically protected conductive surface states.[1] Since the realization of the first 2D TI through HgTe quantum wells,[2] the interest in this class of materials has increased rapidly, with many potential applications proposed in the literature, including charge current to spin current converters for spintronics,[3] high-zT thermoelectrics,[4] high-responsivity photodetectors,[5] low dissipation interconnects,[6] and, if coupled to a superconductor, topological qubits.[7]

In recent years, multiple TIs were identified and extensively studied, such as Bi_2Se_3, Bi_2Te_3, $Bi_{1-x}Sb_x$, $(Bi_{1-x}Sb_x)_2Te_3$, or Sb_2Te_3.[3,8] The issue is that these TIs have relatively small bulk bandgaps, below 0.35 eV,[5,9,10] meaning that the bulk is still a parallel transport channel to the surface states in most cases. Furthermore, in Bi_2Se_3 and Bi_2Te_3, the Fermi energy shifts overtime after the sample preparation, increasing the trivial carrier concentration.[8] Thus, a wide bandgap TI that is stable to air exposure is still being researched.

One of the materials proposed in the literature is the perovskite barium bismuthate, $BaBiO_3$ (BBO). From density functional theory (DFT), this oxide is expected to exhibit a band inversion, characteristic of a TI, in a relatively large gap of ~0.7 eV, which is higher than the TIs extensively studied in the literature. However, the TI gap is about 2 eV above the Fermi energy, requiring either gating or doping the material to access it.[11] More specifically, the addition of one extra electron per unit cell is needed.[12]

To raise the Fermi energy by 2 eV only by gating, a carrier density of about 4×10^{14} cm^{-2} would already be needed for a monolayer of BBO. For a thicker BBO, a carrier density higher than what is achievable in the literature would be needed.[12] For this reason, at least partial doping is required to reach the TI phase in BBO. BBO could be n-doped by substituting Ba with La,[13] Bi with I, or

© Author(s) 2025

Br,[14] Nb,[15] or O with F.[16] Here, we will focus on the fluorination of BBO.

In the literature, different reagents were used to successfully fluorinate oxide perovskites without altering the cation sub-lattice: fluorine gas, transition metal fluorides, XeF_2, ammonium fluoride, and fluorine-containing polymers. An important requirement for a successful fluorination process is good anion mobility in the precursor compound, which, in perovskite materials, usually depends on the presence of anion vacancies. This means that fluorination should be possible in anion-deficient perovskites but also in stoichiometric ones when the cation presents two stable oxidation states that allow the creation of vacancies while the reaction is happening.[17] In BBO, Bi has two available oxidation states,[12] making the fluorination theoretically possible also for this perovskite. This is also supported by the recent literature about the full fluorination of BBO thin films to $Ba_2Bi_2F_5$ by annealing them in an Ar flow in the presence of poly(vinyldene fluoride) or ZnF_2 for up to 24 h.[18,19] The literature also shows that BBO can be fluorinated without altering the cation sub-lattice if the temperature is kept below 250 °C.[18]

Despite this, in the literature, we can also find some concerns about the stability of the perovskite when 33% of oxygen anions are substituted by fluorine, the amount necessary to introduce the required electron per unit cell.[12] In fact, $BaBiO_2F$ is expected to decompose into Bi_2O_3, $BaBiO_{2.5}$, and BaF_2.[20]

In this paper, we discuss the results we obtained using SF_6 plasma, a commonly available gas in the semiconductor industry, to fluorinate MBE-grown BBO thin films on STO/Si(001). In addition, we also prepared substoichiometric BBO_{3-x} films and compared their reactivity to that of the stoichiometric films, since anion vacancies are expected to help in the reaction.[17]

II. METHODS

For this study, 25 nm-thick BBO_3 and BBO_{3-x} thin films were epitaxially grown on silicon (001) substrates by plasma-assisted MBE through a 15 nm-thick $SrTiO_3$ buffer layer.[21,22] To obtain BBO_{3-x} films, the samples were cooled down in vacuum after the growth, while for BBO_3 films, the oxygen plasma was left on during cooling.[23]

Fluorine alloying of the BBO thin films was executed using an APEX SLR HDP-CVD. For the procedure, the process chamber was brought to a temperature of 150 °C and a pressure of 5 mTorr; then, a mixture of SF_6 (50 SCCM) and N_2 (20 SCCM) was introduced into the chamber. To ignite the plasma, the RF power is increased to 100 W and then decreased to 10 W for the duration of the recipe to prevent physically etching the samples, while the inductively coupled plasma (ICP) coil power was kept at a fixed power (300 W for most samples, as discussed in Sec. III). To try to minimize the impact of previous processes on the results, before exposing a batch of BBO film to the plasma, a 10 min chamber conditioning step was executed utilizing the same process parameters of the real exposure process without a sample in the system.

Structural characterization of the BBO samples was carried out by XRD and AFM. For the XRD analysis, a Panalytical X'Pert diffractometer was used, equipped with a Cu K-alpha source and a PIXcel1D detector. AFM images were collected in pulsed force mode using a Bruker ICON PT system and HQ:NSC19/Al BS tips. To evaluate the surface morphology of the samples, the Rq (the root mean square average of height deviations taken from the mean image data plane) of a $5 \times 5\ \mu m^2$ area close to the center of the sample was used.

For the chemical composition study, XPS and TOF-SIMS were used. XPS measurements were carried out using the Al K-alpha (1486.6 eV) x-ray source of a Physical Electronics Versaprobe 3 and a spot size of 100 μm. Charge neutralization and gas cluster ion beam (GCIB) sputter cleaning were used for these measurements. XPS spectra were obtained using an exit angle of 45°. TOF-SIMS characterization used a ION-TOF GmbH TOFSIMS NCS system in a dual beam configuration with a Mn^+ analysis beam (15 keV) and a Cs sputter beam (350 eV).

Finally, the DFT band structure calculations were performed using density functional theory (DFT) as implemented in the CP2K package,[24,25] which employs a hybrid approach combining a Gaussian basis set with an auxiliary plane wave basis set to solve the Kohn–Sham equations. The DZVP-MOLOPT-SR basis sets[26] were used for barium, bismuth, and oxygen atoms, in conjunction with the Goedecker-Teter-Hutter (GTH) pseudopotential.[27] A plane wave cutoff of 900 Ry was applied, ensuring convergence of the total energy. The PBEsol exchange–correlation functional was chosen to mitigate the bond-length overestimation typically observed in generalized gradient approximation (GGA) functionals.[28]

19 March 2026 09:41:09

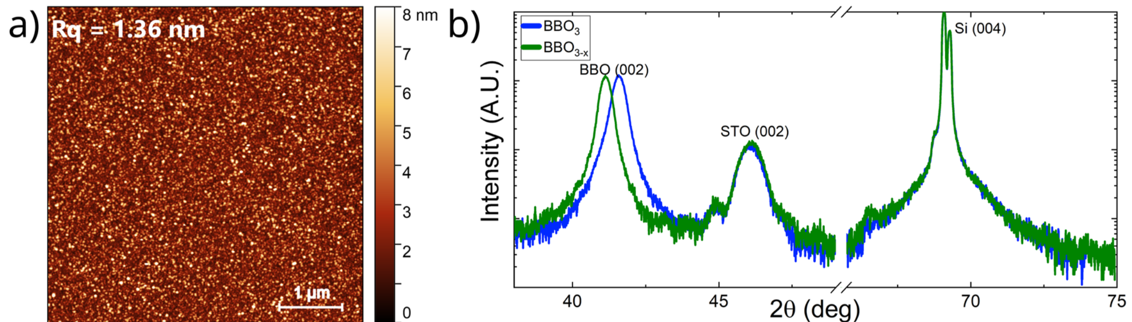

FIG. 1. (a) $5 \times 5\ \mu m^2$ AFM images of a typical BBO_3 sample and (b) $2\theta - \omega$ XRD diffractogram of a BBO_3 (blue line) and a BBO_{3-x} (green line) sample after growth. In the XRD diffractogram, the intensity is normalized to the height of the Si (004) peak.

© Author(s) 2025

III. RESULTS AND DISCUSSION

A. Samples

For this study, we used 25 nm-thick BBO_3 and BBO_{3-x} thin films grown by MBE on Si (001) substrates through a $SrTiO_3$ (STO) buffer layer. The quality of the as-grown samples is shown in Fig. 1. AFM images of different BBO_3 and BBO_{3-x} samples from different growth batches showed a smooth surface morphology with an Rq of about 1 ± 0.2 and 1 ± 0.3 nm, respectively (reported in Fig. S1). As an example, the AFM image of a typical as-grown BBO_3 sample is reported in Fig. 1(a). In a previous study, we showed that quickly cooling down the sample after growth results in a partially oxygen deficient BBO_{3-x}.[29] The $2\theta - \omega$ XRD diffractogram in Fig. 1 confirms that this is also true for the samples used in this study. In fact, for the BBO_{3-x} film, we can extract a lattice parameter c of 4.39 Å, indicating $0.1 < x < 0.37$.[30] For the sample that was slowly cooled down in an oxygen environment, we can compute a smaller lattice parameter c of 4.34 Å, close to the values reported in the literature of 4.334 Å for both powder BBO and[31] BBO films on STO.[18,19,32] In addition, the XRD also confirms the epitaxial relationship between the different layers and, due to the Pendellösung fringes around the BBO and STO peaks, the high quality of the interface between them.

B. Processing conditions

We started our investigation by studying the impact of different processing conditions on the surface morphology of the films. In fact, we are interested in studying the fluorination of BBO for its potential application in TI devices, where the quality of the surface is of critical importance. One batch of BBO_3 and one of BBO_{3-x} were exposed to SF_6 plasma using different ICP powers for different times, and the morphology of the processed samples was studied by AFM. If processing conditions were to cause a significant degradation or etching of the film, a noticeable impact on the surface morphology would be expected. $5 \times 5\ \mu m^2$ AFM images of the BBO_3 samples are displayed in Fig. 2. The Rq of these samples, used to characterize their roughness, is displayed in the insert of Fig. 2, together with the Rq values of the BBO_{3-x} samples and the value of 1 nm typical of as-grown samples. From the AFM Rq data, we can see that BBO_3 and BBO_{3-x} samples show the same trend vs power and time. At 300 W, we see an initial smoothening of the surface followed by an increase in roughness in time, and, after 6–8 min of exposure, the surface morphology of the samples becomes significantly different than that of a pristine sample. From the same figure, we can also see that when the power is increased to 600 or 900 W, the films are completely destroyed already after 2 min of exposure. At these higher powers, we can see the appearance of features thicker than the BBO film, indicating that either the film is being etched or a new phase is being redeposited onto its surface.

C. XRD

While AFM images can be helpful to give a first idea of whether the plasma exposure adversely affects the samples, they do not give any information on the bulk of the films. To assess the impact of the doping process on the BBO lattice, XRD was employed. For this, only the samples processed at 300 W were measured, since the ones at 600 and 900 W already showed clear signs of degradation. The diffractograms are shown in Fig. 3. From the XRD, we can see a degradation in crystallinity in all samples. In particular, a reduction in peak intensity of about 55%, 78%, and 96% can be seen for the BBO_3 samples exposed for 2, 4, and 6 min, respectively. For the BBO_{3-x} samples, a similar trend, with reductions of 46%, 60%, and 96%, is observed. For both BBO_3 and BBO_{3-x} samples, a processing time of 8 min resulted in the full disappearance of the XRD diffraction peak. In addition to the decrease in intensity, from Fig. 3, we can also observe an increase in the out of plane lattice parameter c as the film is exposed to SF_6 plasma. More specifically, c increases from 4.34 to 4.38 Å for BBO_3 and from 4.39 to 4.42 Å for BBO_{3-x}.

Most likely, the observed degradation of crystallinity is caused by the formation of oxygen vacancies in the film due to the low pressure in the processing chamber. Considering that the lattice

19 March 2026 09:41:09

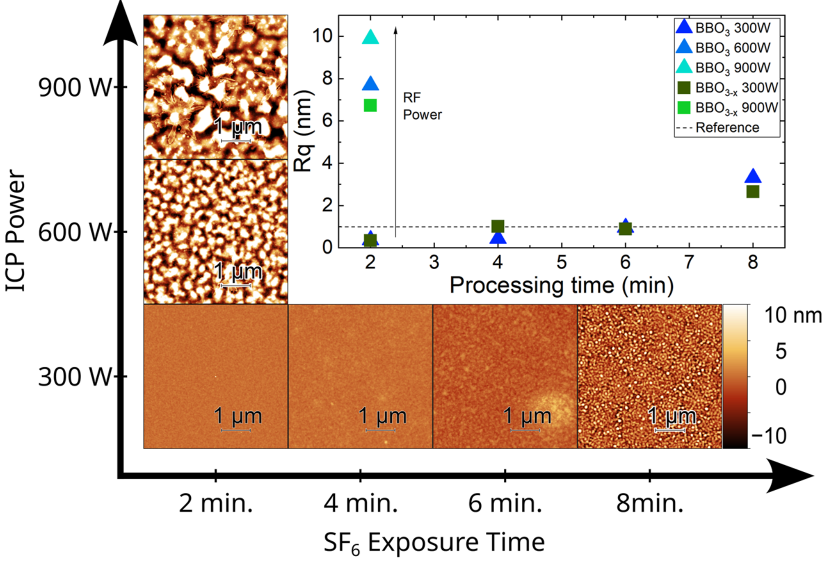

FIG. 2. $5 \times 5\ \mu m^2$ AFM images of BBO_3 samples exposed to SF_6 plasma at different temperatures and ICP powers (scale bar: 500 nm). The color scale is the same for all the AFM pictures. The insert displays the roughness of these samples and of BBO_{3-x} samples processed in the same way. The line in the graph represents the reference value of 1 nm observed for as-grown samples.

© Author(s) 2025

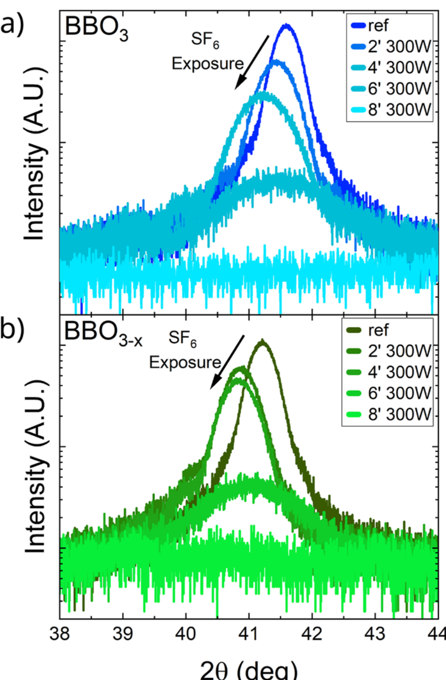

FIG. 3. XRD diffractograms of (a) BBO_3 and (b) BBO_{3-x} samples exposed to SF_6 plasma at 300 W for different times. The intensity has been normalized to the maximum intensity of the Si substrate peak.

parameter of $BaBiO_{2.5}$ is 4.55 Å,[30] the formation of oxygen vacancies is also, at least partially, responsible for the expansion of the BBO lattice. The expected lattice parameter from DFT for $BaBiO_2F$ in the literature is 4.6 Å,[12] so the lattice expansion might also come partially from the incorporation of fluorine into the film, but XRD data alone cannot confirm the presence of fluorine in the film.

D. XPS

To investigate whether the exposure to a fluorine rich environment resulted in the incorporation of fluorine into the BBO structure or just in the formation of oxygen vacancies, XPS was used. For this study, only the reference samples and the ones treated for 2 and 4 min that still presented an XRD peak with a significant intensity were analyzed. Before measuring, the samples were cleaned by GCIB sputtering to remove most of the carbon on the surface. This was done to enhance the signal from the fluorine in BBO (as shown in Fig. S3) but made the calibration less accurate. In fact, it is common practice to calibrate the spectra by shifting the adventitious carbon peak to a reference value, but the cleaning caused the carbon peak to become almost indistinguishable from the background. The XPS spectra were, thus, calibrated using the carbon peak in the spectra before sputter cleaning (placing it at 284.5 eV) and aligning on the Ba $3d_{5/2}$ peaks before and after the GCIB. This procedure likely adds a small shift to the peaks. The survey scans of the reference samples and the samples exposed for 2 min are reported in the supplementary material (Fig. S2). In the survey scans of all the samples, no clear sulfur peak was detected, indicating that, while using SF_6 plasma instead of a pure fluorine plasma probably causes

19 March 2026 09:41:09

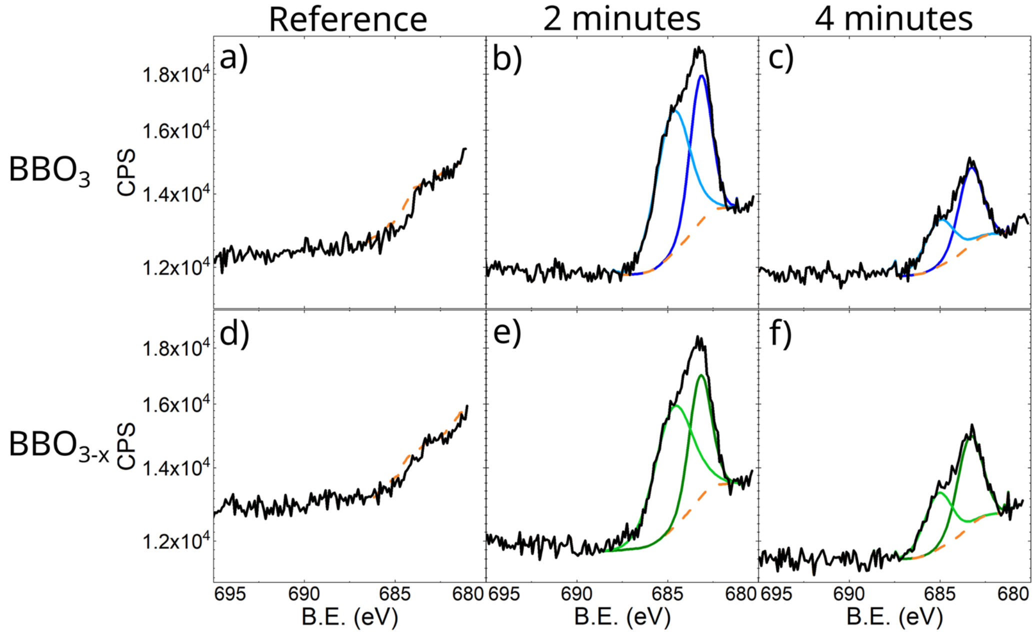

FIG. 4. XPS F 1*s* peaks for the BBO_3 [(a)–(c)] and BBO_{3-x} [(d)–(f)] samples exposed to SF_6 for 0, 2, and 4 min. The black line represents the raw data, the orange line is the baseline used to fit, and the blue and green peaks are the two components into which the peak can be decomposed for BBO_3 and BBO_{3-x}, respectively.

© Author(s) 2025

sulfur contamination in the films, its amount is very limited. In the same scans, we can also notice a peak around 680 eV that could be attributed to either the F 1*s* or the Bi 4*p*3. A higher resolution scan was carried out for all the samples in this region. In these spectra, the Bi peak can be seen for all samples around 680 eV. Only in the treated samples, a second peak attributed to F 1*s* can be observed at about 684 eV. This is reported in Fig. 4. The F 1*s* peak can be decomposed into two components. Considering the small difference in energy between F–Bi[33] and F–Ba[34] bonds, the spread of binding energies for these bonds in pure fluorides according to the databases,[34] and the presence of an additional electronegative element, oxygen, in the BBO system, accurately identifying the chemical environment that gives rise to these two components is not feasible. However, both of these components indicate a bond between fluorine and a metal[34] and are likely due to slightly different oxyfluoride environments in the film. This suggests that the fluorine was successfully introduced into the structure.

From the XPS spectra, we can estimate a concentration of 11 ± 2 and 5 ± 1 at. % for the BBO_{3-x} samples processed for 2 and 4 min and 13 ± 2 and 4 ± 1 at. % for the BBO_3 ones. These values would correspond to ∼18%, 8%, 22%, and 7% of the oxygen substituted by fluorine, respectively.

E. SIMS

The XPS data allowed us to verify the presence of fluorine in the film, but due to the surface-sensitivity of the technique, a different approach is needed to study the fluorine incorporation and distribution in the bulk of the BBO films. For this, new batches of BBO_3 and BBO_{3-x} samples were grown and exposed to the SF_6 plasma at 300 W for 1, 2, 3, and 4 min using the same recipe. As reported in Fig. S4, also for these samples, a decrease in the intensity of the XRD peak coupled to an increase in the out-of-plane lattice parameter can be seen, together with only small variations of Rq roughness by AFM. These samples were measured by TOF-SIMS using Mn^+ as the analysis beam and Cs as the sputter beam. The full Bi^-, Si^-, O^-, and F^- concentration profiles are displayed in Fig. S5. A zoomed in graph of the F^- and O^- profiles in the BBO region is reported in Fig. 5. In both figures, to account for differences in surface roughness, the fluence was multiplied by a value between 1 (for the reference) and 0.94 (for the rougher samples exposed to the plasma for a longer time), aligning the silicon profiles of the samples of the same batch. From this figure, we can clearly see that fluorine was successfully introduced in all the samples. Furthermore, we can also see that all the samples present similar features in the fluorine concentration profile. A peak in concentration can be seen in the first few nm of the BBO film, then the concentration decreases along the thickness, and finally, a second peak is seen at the interface between the BBO and the STO. As we increase the processing time, the initial peak decreases in intensity, and the amount of fluorine diffused into the bulk of the film increases. This can also explain the decrease in fluorine concentration observed between the samples processed for 2 and 4 min by XPS, considering its surface sensitivity. A second piece of information we can gather from Fig. 5 is that the increase in fluorine concentration in the films is coupled to a decrease in oxygen concentration, suggesting that the fluorine is indeed substituting for the oxygen in the BBO structure. Comparing the concentration profiles of BBO_3 with those of BBO_{3-x}, we can also see that in the former, more fluorine accumulates at the interface with STO, while in the latter, it diffuses more into the bulk of the film. This supports the hypothesis that oxygen deficiencies facilitate the fluorination of the film. Using BBO_{3-x} also presents a drawback. In fact, as shown in Fig. S5, in the BBO_{3-x} films, the sharpness of the Bi profile at the BBO/STO interface is degraded by the processing, indicating a lower stability of the film to the processing.

IV. THERMODYNAMICS OF THE FLUORINATION

The XRD data here reported could indicate either the formation of oxygen vacancies or the fluorination of the perovskite upon its exposure to the SF_6 plasma. According to our XPS and SIMS analysis, fluorine was successfully introduced into the BBO layer by the procedure studied in this paper, and, according to the latter, the increase in fluorine concentration was coupled to a decrease in the oxygen concentration. Thus, the data seem to indicate that the SF_6 plasma exposure results in the substitution of the oxygen in BBO with fluorine.

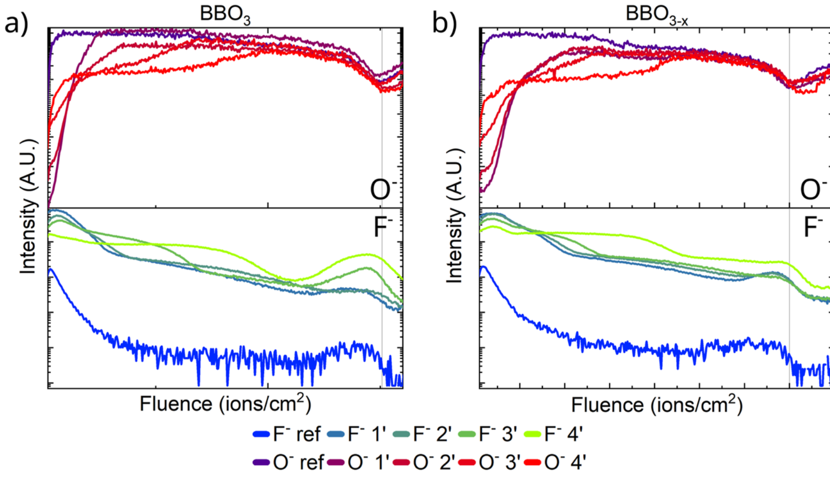

FIG. 5. SIMS O^- and F^- of (a) BBO_3 and (b) BBO_{3-x} and samples exposed to SF_6 plasma for 0, 1, 2, 3, and 4 min. The red shades represent the oxygen concentration profiles, while the blue to green shades represent the fluorine ones. The vertical line represents the position of the BBO/STO interface estimated from the bismuth profile (not shown here).

19 March 2026 09:41:09

© Author(s) 2025

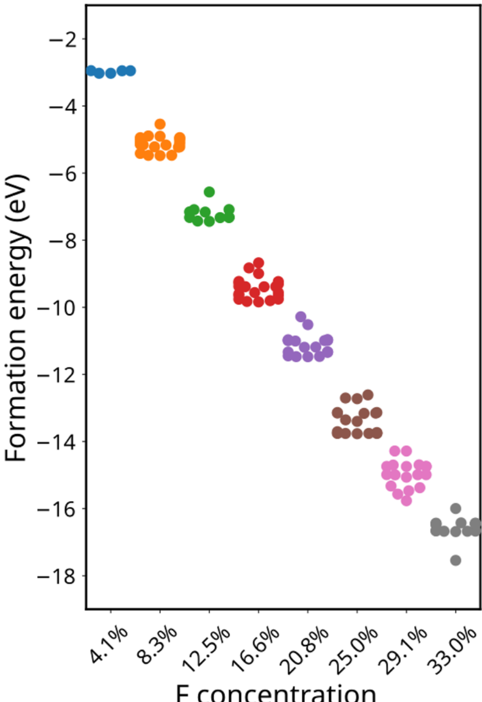

FIG. 6. Formation energy associated with the substitution of oxygen with fluorine in $BaBiO_3$ vs fluorine concentration in the C2/m phase expected at room temperature.[35] The multiple data points at each concentration correspond to the various symmetry-inequivalent fluorine positions within the unit cell.

To support this interpretation, the formation energy associated with the substitution of x oxygen atoms with fluorine was calculated using DFT calculations based on the following equation:[36]

$$E_{f,xF} = E_{tot,xF} - E_{tot,stoi} + x \cdot \mu_O - x \cdot \mu_F, \qquad (1)$$

where μ_O and μ_F are the chemical potentials of oxygen and fluorine, respectively, $E_{tot,xF}$ is the total energy of the substituted structure, and $E_{tot,stoi}$ is the total energy of the stoichiometric structure. The formation energy as a function of fluorine concentration in the BBO structure is shown in Fig. 6. The multiple data points at each concentration correspond to the various symmetry-inequivalent fluorine positions within the unit cell. As illustrated in Fig. 6(b), the formation energy associated with fluorine substitution in the BBO crystalline structure at room temperature is negative, indicating that the process is energetically favorable. Thus, placing a BBO film in a fluorine-rich environment should result in its spontaneous fluorination over time if the mobility of the fluorine in BBO allows it.

V. DISCUSSION

In this paper, we wanted to study the fluorination of BBO films by exposing them to SF_6 plasma. By XRD and AFM, we showed that it is possible to find a set of processing conditions for which the samples are not fully degraded by the plasma exposure, and by XPS and SIMS, we confirmed that fluorine can be introduced into the BBO film.

The fluorination approach followed in this study could be promising due to its speed and scalability. In fact, the fluorination process happens in a few minutes instead of the multiple hours required by the Polyvinylidene difluoride (PVDF) or ZnF_2 method found in Refs. 18 and 19. Furthermore, it uses an SF_6 plasma, commonly available in the semiconductor industries, and a chamber that allows processing on a full wafer, making the process easier to scale. However, it is also important to discuss the main limitations arising from this study.

First, as mentioned in the introduction, to access the topological gap in BBO_3, the Fermi energy needs to be increased by 2 eV. Doing this by fluorine doping alone would mean substituting 33% of the oxygen atoms with fluorine. In this study, only a maximum of ~22% of oxygen was substituted by fluorine. While this amount can probably be further increased by optimizing the substrate temperature and gas flow, it is unlikely to reach the target. However, as we can see from the band structures in Fig. 7, a smaller amount of fluorine can significantly decrease the energy difference between the Fermi energy and the TI gap, making it easier to access with either gating or an additional doping process. Furthermore, while according to DFT, increasing the fluorine concentration allows us to increase the Fermi energy in the material, preserving the band inversion and making it possible to access the TI gap, it also predicts that it causes a bandgap narrowing. Thus, combining the fluorination with another doping or gating might be needed anyway.

Second, from the SIMS concentration profiles, we can see that the fluorine is not distributed uniformly over the thickness of the BBO film. A concentration peak can be seen near the surface, followed by a decrease in concentration and a second peak near the STO/BBO interface. Considering that no cleaning procedure was performed before the measurement, the first peak might be overestimated. In fact, a peak is also visible for the reference sample, in which no fluorine is present. However, an additional annealing step could be required to increase the fluorine mobility in the film and smooth out the peak. Regarding the decrease in concentration along the film thickness, this study used 25-nm-thick films to better study the fluorination process; in real TI devices, the use of thinner films would be beneficial. In fact, to decrease the influence of the bulk as a parallel transport channel, using a film as thin as possible without causing an interaction between the front and the back surface states is recommended. As an example, in Bi_2Se_3, this thickness is around six quintuple-layers, or ~6 nm.[37] If we consider the fluorine profiles in Fig. 5 for the samples exposed to the plasma for 3 and 4 min, we can see that the drop in concentration happens after around 6 and 12 nm. Thus, the concentration drop in the bulk should not be a concern in real applications. In Fig. 5, we can also see that the peak at the interface is much less pronounced in the BBO_{3-x} films compared to the BBO_3 ones.

Third, while processing the samples at 300 W does not fully remove the BBO XRD peak, it does decrease its intensity. Finding a way to reduce or reverse this damage to the crystalline lattice might be important for a practical application of doped BBO. For example, performing an annealing step after the fluorination to improve the BBO crystallinity could be beneficial. In particular, due to the negative formation energy associated with the fluorine substitution, the increased temperature during the annealing step should not cause

19 March 2026 09:41:09

© Author(s) 2025

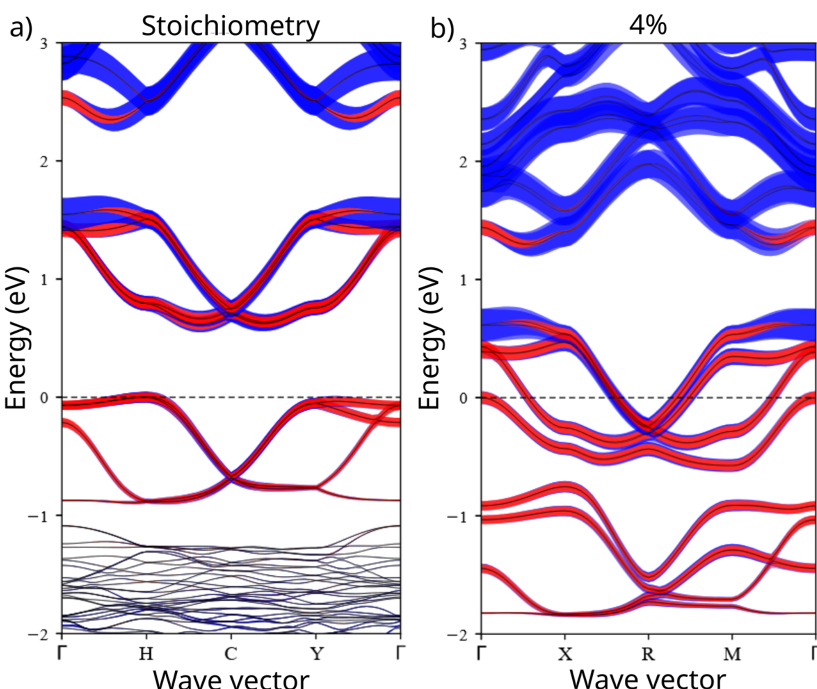

FIG. 7. Band structure of (a) pristine and (b) 4% fluorine doped $BaBiO_3$. The Bi-s character of the band is reported in red, while the Bi-p character is blue. A band inversion can be seen at the Γ point in both cases. The $P2_1/c$ structure, expected at low temperatures,[35] was used to compute the band structures reported here.

the removal of fluorine from the BBO. Furthermore, the increased fluorine mobility during this step might even allow us to get a more uniform fluorine concentration profile.

Finally, if we compare our characterization of the first batch of BBO with those obtained with the second batch, we can see that, while the trends are the same, the exact lattice parameters extracted from XRD after a certain exposure time are not exactly the same. This is likely due to small variations in surface roughness, thickness, and stoichiometry between different growth batches of BBO, combined with the intrinsic variability in some of the process parameters, such as the exact time for the plasma ignition and the pressure in the chamber.

VI. CONCLUSION

In this paper, we explored the low-temperature fluorination of MBE-grown BBO_3 thin films by exposing them to a fluorine-rich environment constituted by a SF_6 plasma in different conditions. Furthermore, we compared the process with the fluorination of oxygen deficient BBO_{3-x} films, expected to be easier to alloy.

We demonstrated by AFM and XRD that, while processing at a high power or for long times results in the full degradation of the BBO layer, a processing region in which the surface morphology and crystallinity are at least partially preserved can be found. We used SIMS and XPS to prove that in this processing window, a significant increase in fluorine concentration in both BBO_3 and BBO_{3-x} can be observed. Furthermore, we also showed that the increase in fluorine content is partially due to the formation of a metal–fluorine bond and that this is coupled to a decrease in oxygen concentration, suggesting that fluorine did substitute for oxygen into the structure. To support this hypothesis, we determined by DFT that the substitution is energetically favorable. Finally, we confirmed that oxygen deficient samples of BBO_{3-x} can be more easily fluorinated than BBO_3 ones, although the BBO_{3-x} seemed to be less resilient to the processing.

SUPPLEMENTARY MATERIAL

The supplementary material to this paper provides a scatter-plot with the spread of roughness of as-grown BBO_3 and BBO_{3-x} films, the XPS survey spectra of the reference and processed samples, a comparison between the F 1*s* spectra of the fluorinated samples before and after GCIB cleaning, the roughness and XRD peak positions and intensity of the samples used for the TOF-SIMS characterization, and the full range of the TOF-SIMS data of Fig. 5 together with the Bi^- and Si^- signals.

ACKNOWLEDGMENTS

The authors would like to acknowledge P. Verdonck for their help in setting up the recipe in the APEX SLR HDP-CVD tool. The authors extend their gratitude also to T. Conard and A. Vanleenhove for XPS operation and R. Tilmann and A. Franquet for operating the TOF-SIMS.

This work has received the funding from the European Research Council (ERC) under the European Union's Horizon 2020 research and innovation program (Grant Agreement No. 864483).

AUTHOR DECLARATIONS

Conflict of Interest

The authors have no conflicts to disclose.

19 March 2026 09:41:09

© Author(s) 2025

Author Contributions

L. Ceccon: Conceptualization (equal); Methodology (lead); Writing – original draft (lead); Writing – review & editing (lead). **I. Ahmed**: Conceptualization (equal); Resources (lead). **M. Kaviani**: Software (lead). **J. Van de Vondel**: Methodology (supporting); Writing – original draft (supporting); Writing – review & editing (supporting). **G. Pourtois**: Software (supporting). **C. Merckling**: Conceptualization (equal); Funding acquisition (lead); Methodology (supporting); Writing – original draft (supporting); Writing – review & editing (supporting).

DATA AVAILABILITY

The data that support the findings of this study are available from the corresponding author upon reasonable request.

REFERENCES

[1] C. L. Kane and E. J. Mele, Phys. Rev. Lett. **95**, 146802 (2005).
[2] M. König, S. Wiedmann, C. Brüne, A. Roth, H. Buhmann, L. W. Molenkamp, X.-L. Qi, and S.-C. Zhang, Science **318**, 766–770 (2007).
[3] J. Yun and L. Xi, Adv. Quantum Technol. **7**, 2400041 (2024).
[4] Y. Xu, Z. Gan, and S.-C. Zhang, Phys. Rev. Lett. **112**, 226801 (2014).
[5] W. Tian, W. Yu, J. Shi, and Y. Wang, Materials **10**, 814 (2017).
[6] T. M. Philip, M. R. Hirsbrunner, M. J. Park, and M. J. Gilbert, IEEE Electron Device Lett. **38**, 138 (2017).
[7] L. Fu and C. L. Kane, Phys. Rev. Lett. **100**, 096407 (2008).
[8] T. Ginley, Y. Wang, and S. Law, Crystals **6**, 154 (2016).
[9] N. H. D. Khang, Y. Ueda, and P. N. Hai, Nat. Mater. **17**, 808 (2018).
[10] W. Liu, V. Stoica, H. Chi, L. Endicott, and C. Uher, J. Alloys Compd. **647**, 50 (2015).
[11] B. Yan, M. Jansen, and C. Felser, Nat. Phys. **9**, 709–711 (2013).
[12] R. L. Bouwmeester and A. Brinkman, Rev. Phys. **6**, 100056 (2021).
[13] M. Talha and Y. H. Jeong, J. Korean Phys. Soc. **76**, 215 (2020).
[14] S.-T. Pi, H. Wang, J. Kim, R. Wu, Y.-K. Wang, and C.-K. Lu, J. Phys. Chem. Lett. **8**, 332 (2017).
[15] J. Ge, W.-J. Yin, and Y. Yan, Chem. Mater. **30**, 1017 (2018).
[16] B. Khamari and B. R. K. Nanda, Mater. Res. Express **6**, 066309 (2019).
[17] O. Clemens and P. R. Slater, Rev. Inorg. Chem. **33**, 105 (2013).
[18] A. Chikamatsu, K. Kawahara, T. Shiina, T. Onozuka, T. Katayama, and T. Hasegawa, ACS Omega **3**, 13141 (2018).
[19] S. Doyle, E. Tewolde Berhane, P. Zou, A. B. Turkiewicz, Y. Zhang, C. M. Brooks, I. El Baggari, H. L. Xin, and J. A. Mundy, ACS Omega **9**, 39082 (2024).
[20] O. I. Malyi, G. M. Dalpian, X.-G. Zhao, Z. Wang, and A. Zunger, Mater. Today **32**, 35 (2020).
[21] I. Ahmed, S. De Gendt, and C. Merckling, J. Appl. Phys. **132**, 225304 (2022).
[22] G. Niu, B. Vilquin, J. Penuelas, C. Botella, G. Hollinger, and G. Saint-Girons, J. Vac. Sci. Technol. B **29**, 041207 (2011).
[23] I. Ahmed, O. Richard, P. Carolan, M. Gambin, L. Ceccon, M. Kaviani, S. D. Gendt, and C. Merckling, "Structural transformation for $BaBiO_{3-\delta}$ thin films grown on $SrTiO_3$-buffered Si(001) induced by an in-situ molecular beam epitaxy cooldown process," Commun. Mater. **6**, 189 (2025); arXiv:2504.18871 [cond-mat.mtrl-sci].
[24] J. VandeVondele, M. Krack, F. Mohamed, M. Parrinello, T. Chassaing, and J. Hutter, Comput. Phys. Commun. **167**, 103 (2005).
[25] M. Guidon, J. Hutter, and J. VandeVondele, J. Chem. Theory Comput. **5**, 3010 (2009).
[26] J. VandeVondele and J. Hutter, J. Chem. Phys. **127**, 114105 (2007).
[27] S. Goedecker, M. Teter, and J. Hutter, Phys. Rev. B **54**, 1703 (1996).
[28] J. P. Perdew, K. Burke, and M. Ernzerhof, Phys. Rev. Lett. **77**, 3865 (1996).
[29] I. Ahmed, M. Korytov, S. Sergeant, T. Nuytten, T. Conard, S. De Gendt, and C. Merckling, APL Mater. **12**, 031105 (2024).
[30] S. Kambe, I. Shime, S. Ohshima, K. Okuyama, and K. Sakamoto, Solid State Ionics **108**, 307 (1998).
[31] D. E. Cox and A. W. Sleight, Solid State Commun. **19**, 969 (1976).
[32] A. Gozar, G. Logvenov, V. Y. Butko, and I. Bozovic, Phys. Rev. B **75**, 201402 (2007).
[33] XPS International, LLC, "International XPS database," https://xpsdatabase.net/; retrieved 9 March 2025.
[34] National Institute of Standards and Technology, "NIST X-ray photoelectron spectroscopy database - SRD 20," retrieved 5 September 2025.
[35] B. J. Kennedy, C. J. Howard, K. S. Knight, Z. Zhang, and Q. Zhou, Acta Crystallogr., Sect. B: Struct. Sci. **62**, 537 (2006).
[36] C. Freysoldt, B. Grabowski, T. Hickel, J. Neugebauer, G. Kresse, A. Janotti, and C. G. Van de Walle, Rev. Mod. Phys. **86**, 253 (2014).
[37] S. Xu, Y. Han, X. Chen, Z. Wu, L. Wang, T. Han, W. Ye, H. Lu, G. Long, Y. Wu *et al.*, Nano Lett. **15**, 2645 (2015).

19 March 2026 09:41:09

© Author(s) 2025